JOURNAL OF PROPULSION AND POWER
Vol. 24, No. 1, January–February 2008

Turbulence Models Assessment for Large-Scale Tip Vortices in an Axial Compressor Rotor

Yangwei Liu,* Xianjun Yu,* and Baojie Liu†
Beijing University of Aeronautics and Astronautics, 100083 Beijing, People's Republic of China

DOI: 10.2514/1.26134

Six turbulence models frequently used in compressor aerodynamics were employed in the detailed numerical investigations of a low-speed large-scale axial compressor rotor, for which the tip flows were measured in detail with stereoscopic particle image velocimetry, to assess the predictive capabilities of the turbulence models for large-scale vortices in the tip region of the rotor. The six turbulence models include: the mixing-length model, the Spalart–Allmaras model, the standard $k-\varepsilon$ model, the shear-stress transport $k-\omega$ model, the $\overline{v^2}-f$ model, and the Reynolds stress model. Their results were carefully discussed and compared with the measurements both on velocity fields and turbulence stresses. It was found that the Reynolds stress model is superior to the others in the prediction of the tip-leakage vortex at the design condition, whereas the standard $k-\varepsilon$ model shows the best results in the prediction of the corner vortex at the near-stall condition. Although the simulation could predict the large-scale tip vortices well in the mean flowfield, the computed flow mechanism has large discrepancy with the reality.

Nomenclature

A	=	compressor axial direction
H	=	distance from the hub to the tip in the radial direction
p	=	static pressure
R	=	compressor radial direction
T	=	compressor tangential direction
u, v, w	=	mean velocity components in the x, y, and z directions
X	=	distance from the rotor suction surface in the x direction
x, y, z	=	Cartesian coordinates
Y	=	distance from the rotor hub in the y direction
y^+	=	nondimensional turbulence wall function
ν	=	kinematic viscosity
ρ	=	fluid density
ω	=	vorticity

Subscript

c	=	the center of the tip-leakage vortex

Superscripts

$\bar{}$	=	time average
$'$	=	fluctuating quantity

I. Introduction

ROTOR tip flows have a large impact on pressure rise, efficiency, and stability [1–3] and are therefore of great engineering importance when designing axial fans and compressors. Many efforts have been made on the tip flows by theoretical models [2,4–6], experimental investigations [7–14], and numerical simulations [15–19] under various conditions during the last 50 years. Recently, some flow control techniques have also been tried to improve the rotor tip flow performance [20,21]. By the investigations, basic structures and characteristics of rotor tip flow were well-summarized, and thus their main influences on compressor performance have been taken into account in the design and have made a big contribution in the increasing performance of fans and compressors. This has been especially true in the last 20 years, because the steady computational fluid dynamics (CFD) technique has been widely used and has played an increasingly important role in the aerodynamic design routine of fans and compressors. In the near future, the performance of axial fans and compressors will take a further step to support the development of the next generation of high-power-density aeroengines, which require the steady CFD technique used in the design routine that could credibly predict all of the main flow structures and their mechanisms in the blade passage to minimize the design risk.

The tip flows are characterized by complex large-scale vortices, such as the tip-leakage vortex (TLV) and the corner vortex (CV), three-dimensional shear layers, and shock waves in a high-speed condition. Hence, it is still a great challenge for numerical simulations to accurately predict the tip flows due to complicated flow structures. In the future, the general trend in turbomachinery computational fluid dynamics may be toward reducing the use of turbulence modeling through DES or LES. However, only the steady and unsteady simulation solving the RANS equations are currently practicable, and only the steady simulation is popular in the compressor design routine, due to the limitations in computing resources and the design schedule.

Several factors such as turbulence modeling, grid topology/resolution, and tip-clearance modeling would most affect the predictive accuracy for the tip flows. Glanville [22], Van Zante et al. [23], and Gupta et al. [24] systematically compared the various approaches and provided recommendations on required grid topologies/resolutions and tip-clearance modeling. Lee et al. [25] assessed three turbulence models for the tip-leakage flow (TLF) in a linear compressor cascade and an axial-flow fan without high resolution of the grid. Because the turbulence model is currently the main weakness in the CFD of compressor aerodynamics and it is generally accepted that no single turbulence model is universally superior for all classes of problems, systematic studies focused on the performance of different turbulence models in such a situation should be conducted. However, due to the lack of detailed measured results in the rotor blade passage, the assessment of turbulence models is nearly impossible, especially for the most important distributions of the turbulence stresses. Hence, this study attempts to systematically investigate the performance of turbulence models for the prediction of rotor tip flows with steady simulation.

Received 24 June 2006; revision received 31 July 2007; accepted for publication 20 August 2007.

*Ph.D. Student, Group 404, National Key Laboratory on Aero-Engines, School of Jet Propulsion.

†Professor, Group 404, National Key Laboratory on Aero-Engines, School of Jet Propulsion.

Recently, Liu et al. [26] investigated the flows near the tip region inside the rotor passage of an axial compressor test by using stereoscopic particle image velocimetry (SPIV). The measurements could provide abundant data for the complicated tip flow, which are sufficient for the qualitative assessment of turbulence models. In the current investigation, the calculations with six turbulence models frequently used in compressor aerodynamics are compared with the detailed SPIV measurements at both the design and the near-stall conditions. Along with detailed comparisons of both velocity fields and turbulence stresses, the assessment of the turbulence models focuses on their predictive capabilities on the dominant large-scale tip vortices such as the TLV and the CV. The comparisons are valuable for the proper use of the turbulence models, allowing the designers to further understand the numerical results and contributing to the modification of the turbulence models and the development of zonal modeling, etc.

II. Experiment Details

An experimental investigation was conducted by using SPIV on a low-speed large-scale axial compressor facility at Beijing University of Aeronautics and Astronautics. The detailed parameters of the test compressor are summarized in Table 1 and its performance line is shown in Fig. 1. In this study, measurements were conducted at both the design point (mass flow coefficient of 0.58) and the near-stall point (mass flow coefficient of 0.39), respectively.

The layout of the measurement cross sections is shown in Fig. 2. Near the blade suction surface, the measurement planes perpendicular to the blade tip chord are uniformly arranged from 20% of the chord downstream of the blade leading edge to 10% of the chord downstream of the blade trailing edge with an interval of 10% chord length. Near the blade pressure surface, the measurement planes also perpendicular to the blade tip chord are uniformly arranged from the blade leading edge to the blade trailing edge with an interval of 10% chord length. The effective field of view covers about 50–70% of the blade span height and nearly half of a blade passage at both the suction surface and the pressure surface.

At least 100 instantaneous realizations are recorded at each cross section, which yields the ensemble-averaged velocity with an accuracy of about 2, 6, and 3% in the mainstream region, in the tip region, and at the region below 60% of the blade spans, respectively. In the mainstream region, the uncertainties of the turbulence normal stresses are 17–22%, and the uncertainties of the turbulence shear stresses are 25–30%. However, at the near-tip region, they increase to about 30 and 35%, respectively. As discussed by Liu et al. [26], the total 100 images are inadequate to obtain accurate turbulence statistics; however, the statistical results are useful for qualitative analyses of the turbulence characteristics in the test rotor and for the evaluation of turbulence models.

A detailed discussion of the experimental facility, measurement technique, and measurement accuracy is given in a previous paper [26]. More details about the flow in the test compressor, such as the mechanism of the formation, development, and evolution of the TLV, as well as the formation and evolution of the CV, have also been discussed in previous papers [13,14].

III. Numerical Calculation Method

The measurement is conducted within a three-row configuration, and so a multistage unsteady solution with a highly resolved grid

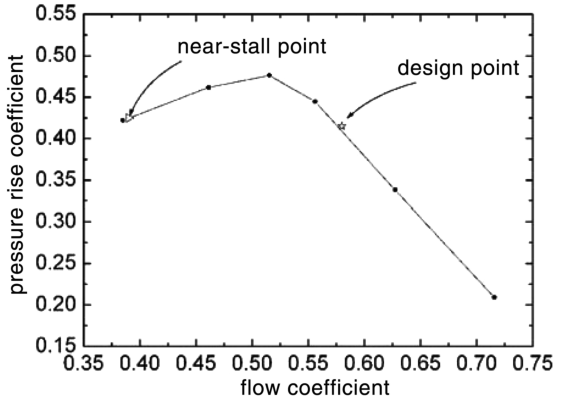

Fig. 1 Compressor characteristic.

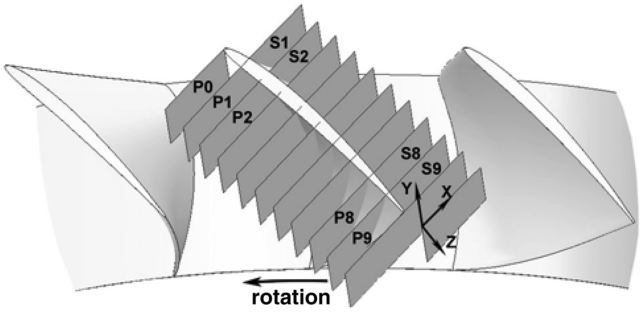

Fig. 2 Schematic layout of SPIV measurement cross sections.

seems to be the preferred method. However, such simulations are still too expensive, especially in the design routine. It will also cause errors from the adjacent blade rows if the predicted flow structures in the adjacent blade rows differ from the realities. Meanwhile, the unsteady blade row interactions are weak because of low blade loads and large axial gaps between blade rows, and a multistage steady solution may cause more errors from the adjacent blade rows with the mixing-plane method. Hence, a steady simulation with the isolated rotor blade was conducted to predict the tip-clearance flow and to avoid expensive cost and errors from the adjacent blade. The inlet and exit of the computational domain were both situated one chord length upstream and downstream of the blade, respectively. The boundary conditions, which were derived from solving the steady three-dimensional RANS equations with the mixing-plane method for the compressor, were also based on the previous measurements so that the boundary conditions at the rotor inlet and exit are nearly accurate.

To minimize the effects of other factors as mentioned before, it would be preferred to assess different turbulence models with the same numerical platform and the same grid. In this way, the differences in the results can be attributed mostly to the differences of the models, and the turbulence model performances can be assessed in a systematic manner. The mature commercial flow solver package FLUENT has thus been employed to solve the flowfield in the compressor rotor with the same grid at both the design and the near-stall conditions. The convergence required that the scaled residuals decrease to 1.0E-6 for all equations.

Table 1 Parameters of the test compressor

Outer diameter, m	1.0	Configuration	IGV + rotor + stator
Aspect ratio	0.6	Number of blades	36 + 17 + 20
Design Speed, rpm	1200	Blade camber angle, deg	17.4 + 26.5 + 49.1
Design mass flow rate, kg/s	22.4	Blade stagger angle, deg	10.4 + 33.4 + 12.3
Flow coefficient	0.58	Blade height, mm	200 + 199 + 198
Pressure rise coefficient	0.4	Blade chord, mm	100 + 180 + 180
Reynolds number rotor tip chord	7.5×10^5	Rotor tip clearance, mm	1.0
Inlet guide vane rotor axial gap, mm	41.9	Rotor–stator axial gap, mm	48.7
Blade type	C4	Vortex design	Free vortex

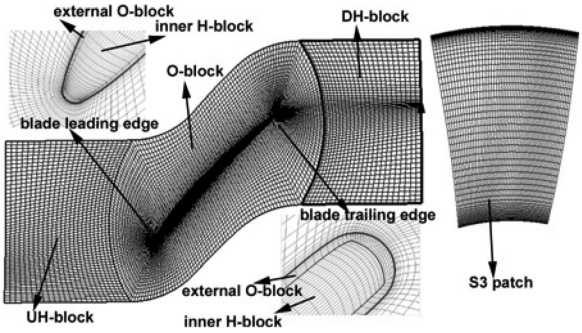

Fig. 3 Grid distribution.

A. Computational Grids

It is well known that sufficient grid resolution is very important for the simulation of the TLF. As indicated by Basson and Lakshminarayana [27], the TLF can exert influence upon a region of approximately $10 \sim 30\%$ of the span from the casing, and therefore a further increase in the grid resolution in the tip region (within about eight tip gaps from the endwall) could provide a more accurate prediction of the TLF. Van Zante et al. [23] recommended that sufficient grid clustering near the casing should be used to accurately resolve the wall-bounded shear layer that impacts the trajectory of the TLF. Gupta et al. [24] also indicated that high-resolution, fully gridded, tip regions could provide a more accurate estimation of the strength of the TLF and its trajectory than any approximate tip model. Their works emphasized the importance of the high resolution of the grids in the radial direction. As discussed herein, enough grid resolution in the circumferential direction is also important for the accurate prediction of the TLF.

The computational grid used in the current investigation was generated with the IGG software package developed by Dener and Hirsch [28]. Referring to the preceding discussions, significant efforts for the grid generation were made to minimize the grid impacts. A multiblock strategy was used to ensure the grid quality and make the grid fully matched. As shown in Fig. 3, it consists of five blocks. The blade passage consists of three blocks, using an H-O-H grid: the upstream UH-block, the O-block around the airfoil, and the downstream DH-block. In addition, the tip gap has two blocks with an inner H-block and an external O-block.

Sufficient grid clustering was specified in the tip region. As shown in Fig. 3, the grid distributions in both the spanwise and pitchwise directions were carefully refined in the tip region. It is well known that the grid resolution should be high enough in the blade boundary layer; hence, the distance between the first grid line and the solid wall was set to $y^+ < 1$ in the computation.

A series of grids were generated with different grid densities and distributions to check the grid independence of the solution. Here, four different grids are presented, the detailed information of which is shown in Table 2.

B. Boundary Conditions

The flow was assumed to be steady and fully turbulent in the computation. The profiles of total pressure, total temperature, and inlet flow angle were specified for the inlet boundary, whereas the profile of static pressure was specified for the outlet boundary. At the inlet, the turbulence intensity and length scale were specified and the Reynolds stresses could be derived from the assumption of an isotropic turbulence. At the outlet, the turbulence intensity and hydraulic diameter were specified. Moreover, nonslip and adiabatic conditions were adopted for all of the solid walls. Periodic conditions were imposed along the pitchwise boundaries.

C. Numerical Scheme and Turbulence Model

A second-order upwind scheme and the central-differencing scheme were used for the convection terms and the viscous terms of each governing equation, respectively, to minimize the numerical diffusion. The pressure–velocity coupling was handled by the SIMPLE algorithm. More detailed descriptions of the numerical scheme can be found in the FLUENT user's manual [29].

Six different turbulence models, including the mixing-length model (ML) [30], the Spalart–Allmaras model (SA) [31], the standard $k-\varepsilon$ model (SKE) [32], the shear-stress transport (SST) $k-\omega$ model [33], the $\overline{v^2}-f$ model (V2F) [34], and the Reynolds stress model (RSM) [35], which are very typical and widely used in the field of turbomachinery, were assessed in the research. The first five models employ the Boussinesq hypothesis to relate the Reynolds stresses to the mean velocity gradients, whereas the RSM solves the transport equations for each term in the Reynolds stress tensor. The advantage of the Boussinesq hypothesis is the relatively low computing cost associated with the calculation of the turbulent viscosity, whereas the RSM is superior in a situation in which the anisotropy of turbulence has a dominant effect on the mean flow.

Enhanced wall treatment [29], which is a near-wall modeling method that combines a two-layer model with enhanced wall functions, was used to represent the turbulent flow in the near-wall region for the SKE and RSM, because they are primarily valid for turbulent core flows (i.e., the flow in the regions somewhat far from walls). If the near-wall mesh is fine enough to be able to resolve the laminar sublayer (typically, $y^+ \approx 1$), then the enhanced wall treatment will be identical to the traditional two-layer zonal model and the wall functions will not be used. Thus, in the current investigation, this treatment can possess the accuracy of the standard two-layer model in the near-wall region, due to the fine near-wall meshes used in the simulations.

D. Discussion of Grid Independence

It is well known that the assessment of the turbulence models should be based on the results with grid independence. The rotor operating characteristics are often used to estimate the grid independence in open literature, but research has found that this cannot ensure the invariability of the specific flow structures such as the TLV and the CV.

Figure 4a shows the calculated rotor operating characteristics in terms of the static pressure rise versus the flow coefficient for the three different grids used. The three lines are nearly identical, and so it seems that the grid independence could be achieved even with the coarsest grid. However, Fig. 4b presents the calculated streamwise vorticity in the core of the TLV at the near-stall condition. The difference between case 1 and the other two is remarkable, whereas the results for case 2 and case 3 are nearly identical. Comparisons of the other flow structures for the three different grids also demonstrated that the results of case 2 and case 3 should be grid-independent. To further confirm the grid independence, simulations have also been conducted using grid case 4 at the design and near-stall conditions. The results for case 3 and case 4 are nearly the same. From the comparisons, it can be concluded that grid-independent results were achieved. To ensure the reliability for the prediction of

Table 2 Mesh distribution information (pitchwise by spanwise by streamwise)

	Passage cell count			Tip cell count		Total cell count
	UH-block	O-block	DH-block	O-block	H-block	
Case 1	$57 \times 73 \times 25$	$29 \times 73 \times 233$	$57 \times 73 \times 25$	$9 \times 17 \times 233$	$25 \times 17 \times 93$	776,485
Case 2	$57 \times 81 \times 25$	$41 \times 81 \times 233$	$57 \times 81 \times 25$	$9 \times 21 \times 233$	$25 \times 21 \times 93$	1,097,505
Case 3	$57 \times 97 \times 25$	$49 \times 97 \times 233$	$57 \times 97 \times 25$	$9 \times 25 \times 233$	$25 \times 25 \times 93$	1,494,449
Case 4	$57 \times 117 \times 33$	$57 \times 117 \times 233$	$57 \times 117 \times 33$	$9 \times 33 \times 233$	$25 \times 33 \times 93$	2,139,957

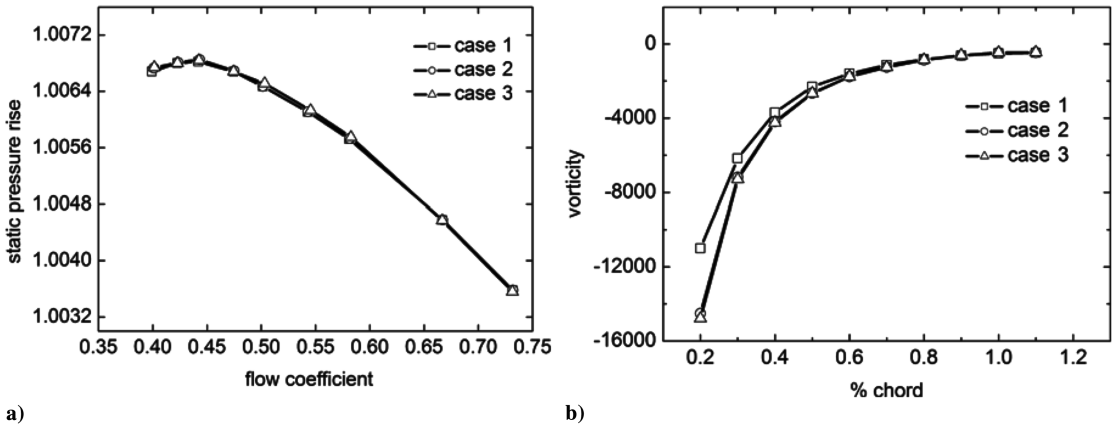

Fig. 4 Plots of the a) static pressure rise and b) streamwise vorticity at the center of the TLV along the vortex trajectory for the near-stall condition.

the complex fine-scale structures, the grid for case 3 was employed in the final calculation.

E. Vortex Identification

The vortex core should first be identified correctly to access the capabilities and limitations of the turbulence models for the prediction of the TLV. There are several popular local vortex identification criteria; however, no single criterion is universally accepted as being superior for all classes of problems. Chakraborty et al. [36] analytically explored the interrelationships between different criteria based on pointwise analysis of the velocity gradient tensor and indicated that all of the criteria can identify the same vortex core region by using the proposed threshold for the intense streamwise vortex. In this study, the $-\lambda_2$ criterion was used in the identification of the TLV and the comparison between the computational and the experimental results. It is simplified into the following two-dimensional incompressible form:

$$\lambda_2 = (\partial u/\partial x)^2 + (\partial v/\partial y)^2 + 2(\partial u/\partial y)(\partial v/\partial x) \qquad (1)$$

The center of the TLV is indicated by the minimum value of λ_2 in its core region. The trajectory of the TLV shown in the following figures is the line passing through the center location of the TLV in each section.

IV. Results and Discussion

The SPIV measured results clearly showed that the TLV arises at both the design and near-stall conditions, whereas the CV only arises at the near-stall condition. Furthermore, the TLV and the CV are the only two large-scale vortices in the tip region of the rotor. More details about the flow mechanism in the test rotor, such as the formation, development, and evolution of the TLV, as well as the CV, can be found in the previous papers [13,14].

The discussion here will focus on the predictive capability of the six turbulence models on the TLV and the CV by comparing with the measured velocity and turbulence stress distributions. The results for the ML are neither shown nor discussed here, because it fails to predict the TLV and the CV correctly. Because of the space limitation, only some representative data at typical streamwise locations are shown and discussed in the later sections.

All of the following analyses are in the relative frame fixed to the rotor. It should be noted that the measured results do not include the casing-wall boundary layer, because of the laser reflection and the seeding pollution. Hence, the fields of the calculated results are a little larger than the measured results.

A. Prediction of the Tip-Leakage Vortex

Figure 5 shows the distribution of the streamwise velocity in the rotor frame at the design condition, whereas Fig. 6 shows the results at the near-stall condition (the planes in Figs. 5 and 6 are the same as those in Fig. 2.). Bold dashed lines in the figures indicate the

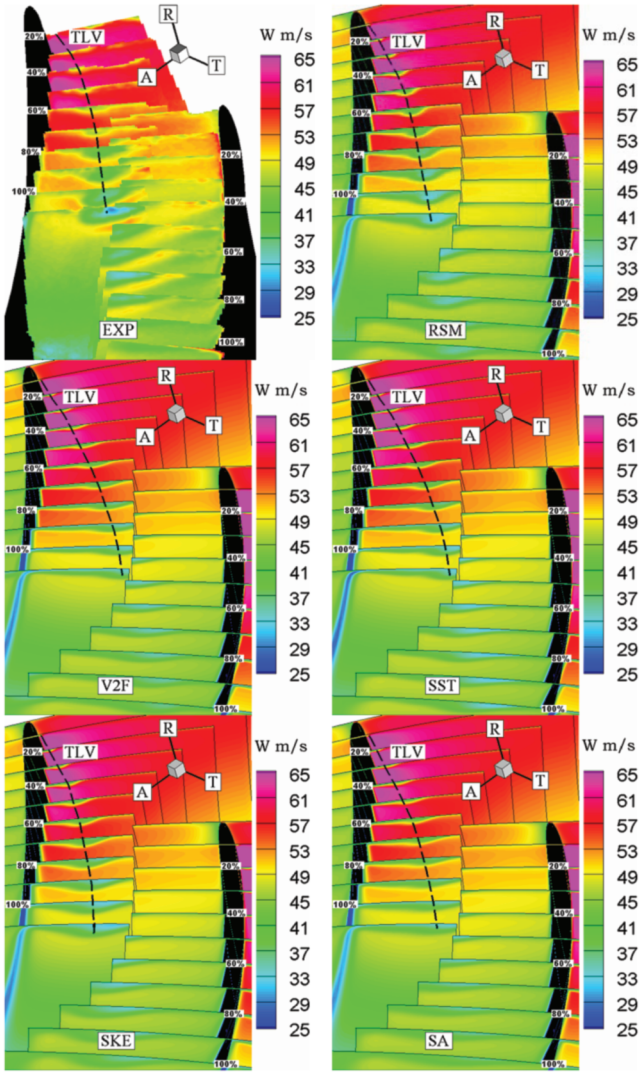

Fig. 5 Composite maps of streamwise velocity distributions for the design condition.

trajectory of the TLV. The vorticity distribution (not shown) with high negative value (the rotating direction of the vortex is opposite to the rotor) in the TLV is similar to the streamwise velocity. According to the distribution of the streamwise velocity in the measurements and the calculations, it can be seen that the TLV expands and the vortex core moves away from both the suction surface and casing wall as the TLV propagates downstream. The interactions of the TLV, the mainstream, and the casing-wall boundary layer, as well as

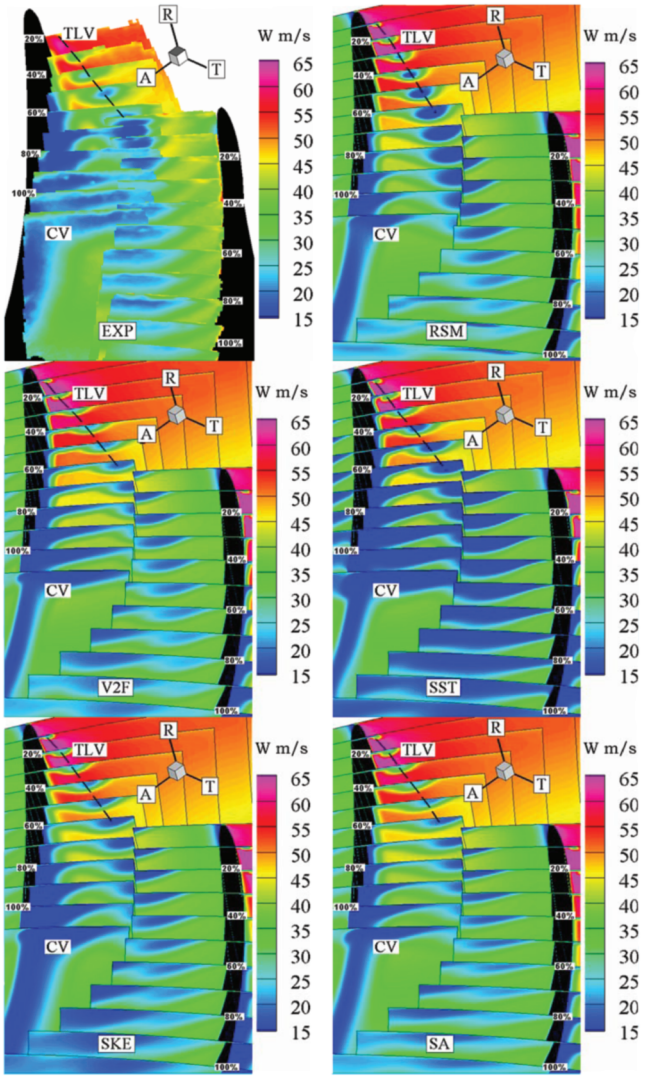

Fig. 6 Composite maps of streamwise velocity distributions for the near-stall condition.

the strong adverse pressure gradient, could accelerate the expansion of the TLV. Comparing Fig. 5 with Fig. 6, it can be seen that the TLV forms earlier at the near-stall condition, with lower streamwise velocity and higher negative vorticity (not shown) in the vortex core. Figure 7 shows the positions of the center of the TLV. As the TLV propagates downstream, its center gradually moves far away from the blade suction surface and the growth of X_C, where X_C is the distance of the vortex center from the rotor suction surface, almost obeys a linear relation with the streamwise distance. The larger gradient of the lines in Fig. 7b indicates that the center of the TLV moves further away from the suction surface at the near-stall condition.

As shown in Figs. 5 and 6, all five turbulence models can predict the formation and development of the TLV, but their difference is evident. At the design condition, the structure, strength, and trajectory of the TLV predicted by the RSM show more agreement with the measurement and are much better than those of the other four turbulence models. At the near-stall condition, the form and strength of the TLV predicted by RSM is still the best, whereas the trajectory of the TLV predicted by V2F and SST shows more agreement with the measurement. The streamwise velocity along the trajectory of the TLV predicted by all five turbulence models varies smoothly and is different from the measurements. According to the measurements, the variation of the streamwise velocity is evidently affected by the TLV splitting or breakdown and the flow becomes complicated [26]. As shown in Figs. 5 and 6, the TLV splitting or breakdown also affects the structure of the TLV in the mean flowfield; hence, the predicted state of the TLV differs largely with the measurement in the rear part.

As shown in Fig. 7, no turbulence model could credibly predict the circumferential motion of the TLV at both the design and near-stall conditions. At the design condition, RSM and SA give the same result in the prediction of the circumferential motion of the TLV and show more reasonable agreement with the measurement, whereas V2F and SST overestimate and SKE underestimates the circumferential motion of the TLV. At the near-stall condition, V2F and SST predict the circumferential motion of the TLV best, whereas other models underestimate the circumferential motion, and SKE is a little better than RSM and SA. From the preceding discussions, it can be concluded that the predictions of the structure and the circumferential motion of the TLV do not seem entirely related. In fact, the prediction of the circumferential motion of the TLV is related to the prediction of the TLV itself and the prediction of the CV that will be discussed in Sec. IV.B.

It is well known that the predictive capability for turbulence stresses plays an important role in the performance of a turbulence model. Usually, a flow solver can exactly predict the mean flow if the turbulence model can predict the turbulence stresses exactly or it can predict well if a turbulence model can predict the primary components of turbulence stresses well. However, the turbulence stresses predicted by different models have different discrepancies from reality. Therefore, the predicted turbulence stresses are compared with the measurements to find the discrepancies. Through the comparisons, we can find the predictive capabilities of turbulence models and better understand them. Figures 8–11 show the distributions of the streamwise vorticity and the turbulence stresses relating to the streamwise velocity fluctuation at the 60% chord for the design condition. The core region of the TLV possesses not only

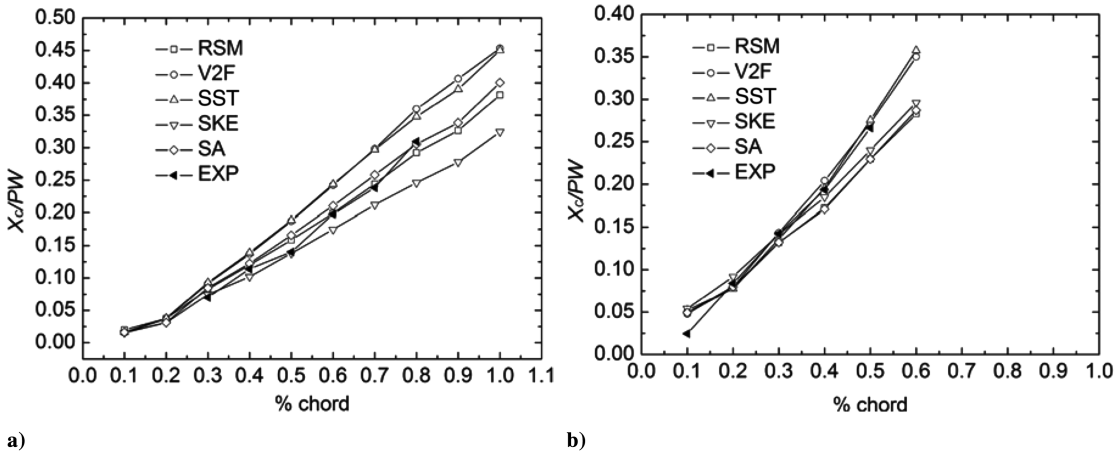

Fig. 7 Center location of the TLV for the a) design condition and b) near-stall condition (PW is the blade passage width normal to the blade tip chord).

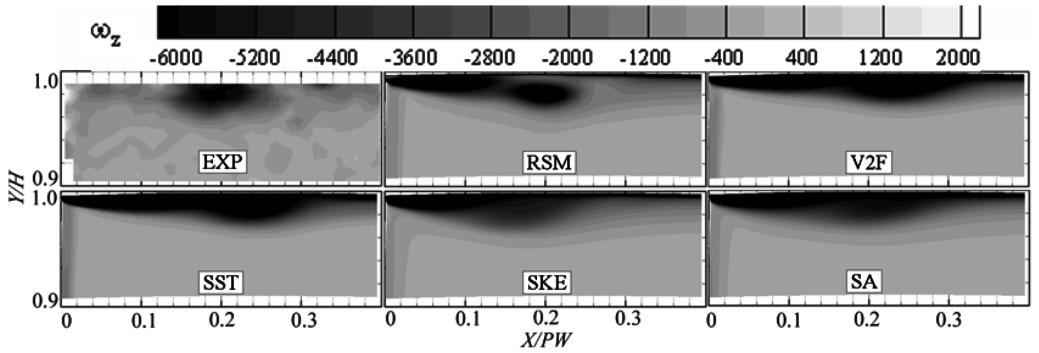

Fig. 8 Streamwise vorticity at 60% chord for the design condition.

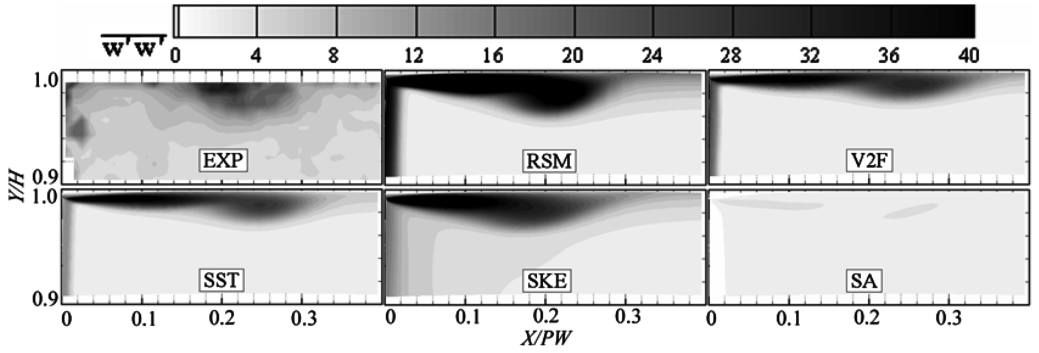

Fig. 9 Normal stress $\overline{w'w'}$ at 60% chord for the design condition.

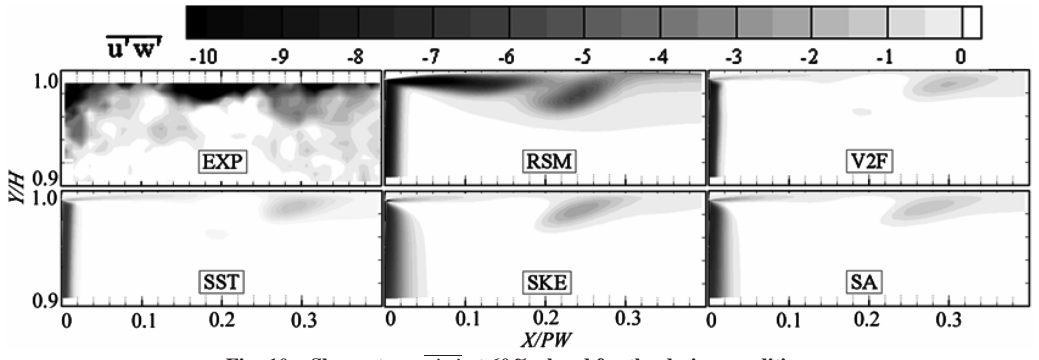

Fig. 10 Shear stress $\overline{u'w'}$ at 60% chord for the design condition.

the high-vorticity, but also the high-turbulence, stresses. As shown in Fig. 8, only the RSM could predict the TLV as an isolated vortex, which would agree well with the measurement. The shear layer of the TLF appears very thick in all of the predicted results, whereas it is very thin in the measurement.

The measured normal stress $\overline{w'w'}$ with high value in the TLV, as shown in Fig. 9, indicates that the streamwise velocity fluctuates distinctly. This phenomenon could be well predicted by all of the turbulence models except SA. However, the stress form and location predicted by RSM agrees best with the experiment. The distributions of normal stress $\overline{u'u'}$ and $\overline{v'v'}$ are similar to that of $\overline{w'w'}$. Comparing the distributions of different normal stresses in the TLV, it can be found that $\overline{u'u'} \geq 2\overline{v'v'} \approx 3\overline{w'w'}$ for the measurement, $\overline{w'w'} \geq \overline{u'u'} \geq 2\overline{v'v'}$ for the prediction with RSM, and $\overline{w'w'} \approx \overline{u'u'} \approx \overline{v'v'}$ for the predictions with the other models.

The measured shear stress $\overline{u'w'}$ and $\overline{v'w'}$ in the TLV, as shown in Figs. 10 and 11, have much lower values than the normal stresses. The shear stress $\overline{u'w'}$ predicted by RSM does not agree very well with the measurement, but is much better than that predicted by the other models. The shear stress $\overline{v'w'}$ predicted by all of the turbulence models agrees well with the measurement. The shear stress $\overline{u'v'}$ with negative value is similar to $\overline{v'w'}$ in the TLV. Comparing the distributions of different shear stresses in the TLV, it can be found that $|\overline{u'v'}| > |\overline{u'w'}| \approx |\overline{v'w'}|$ for the measurement, $|\overline{u'v'}| > |\overline{u'w'}| \approx |\overline{v'w'}|$ for the prediction with RSM, and $|\overline{u'v'}| > |\overline{v'w'}| \gg |\overline{u'w'}|$ for the predictions with the other models.

At other sections in the tip region, the turbulence stresses have similar distributions and the normal stresses are always higher than the shear stresses in the TLV at both the design and the near-stall conditions.

B. Prediction of the Corner Vortex

The measured results in Figs. 5 and 6 show that the occurrence of the CV at the near-stall condition is the primary difference in the rotor tip flow compared with the flows at the design condition. Unlike the TLV, the CV is a compound vortex with its vortex core composed of multiple vortices and its core fluid mainly coming from the boundary layer of the suction surface [13]. At the rotor exit, the low-speed CV occupies nearly one-half of the rotor passage and contributes primarily to the blockage and loss of the flow in the rotor tip region at the near-stall condition.

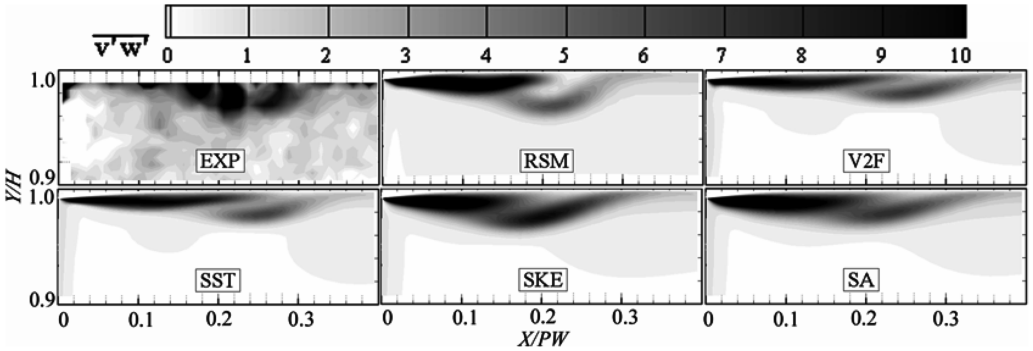

Fig. 11 Shear stress $\overline{v'w'}$ at 60% chord for the design condition.

Figure 6 also shows that all five turbulence models can predict the formation, development, and evolution of the CV. However, the CV predicted by SKE shows a more reasonable agreement with the measurement than those predicted by other turbulence models, especially near the blade suction surface. The SST also shows a better performance in the CV prediction near the casing wall, and the result predicted by V2F shows a somewhat better agreement than those predicted by RSM and SA. It also can be seen that all of the turbulence models except for the SKE underestimate the CV in scale, compared with the measurement. The CV predicted by all five turbulence models seems to be a single vortex, which is different from what the measurements indicate. According to the measurements, the CV is a compound vortex with its vortex core composed of multiple vortices [13].

As discussed in Sec. IV.A, the prediction of the CV affects the prediction of the circumferential motion of the TLV. As shown in Fig. 7, V2F and SST overestimate the circumferential motion of the TLV at the design condition, whereas they predict the circumferential motion of the TLV well at the near-stall condition. This is because V2F and SST underestimate the CV at the near-stall condition, which counteracts the overestimation of the circumferential motion of the TLV compared with that at the design condition. In fact, all of the turbulence models except SKE underestimate the circumferential motion of the TLV at the near-stall condition, compared with that at the design condition. In other words, the occurrence of the CV at the near-stall condition makes it more complicated and difficult to predict the TLV trajectory.

Figures 12–15 show the distributions of the streamwise velocity and the turbulence stresses relating to the streamwise velocity fluctuation at 70% of the chord for the near-stall condition. As shown in Figs. 13–15, the turbulence stresses in the CV are as high as those in the TLV, which also indicate that the unsteadiness of the CV is evident. Compared with the case of the TLV, the turbulence stresses in the CV are harder to predict. SKE can predict the stress structure well, whereas others models except SA can only predict the stress structure reasonably well with an apparent smaller region. The normal stresses $\overline{u'u'}$ and $\overline{v'v'}$ are similar to $\overline{w'w'}$. In the CV, it can be found that $\overline{w'w'} \geq 1.2\overline{v'v'} \geq 2\overline{u'u'}$ for the measurement, $0.5\overline{w'w'} \geq 1.2\overline{v'v'} \geq 2\overline{u'u'}$ for the prediction with RSM, and $\overline{w'w'} \approx \overline{u'u'} \approx \overline{v'v'}$ for the predictions with the other models.

Figures 14 and 15 indicate that the measured shear stresses $\overline{u'w'}$ and $\overline{v'w'}$ are lower than the normal stresses in the CV. SKE can predict the structure of shear stress $\overline{u'w'}$ well, whereas others models including SA only can predict the stress structure reasonably well with an apparently smaller region. In the prediction of the shear stress $\overline{v'w'}$, only RSM results in the same sign as the measurement and other models fails to do so. The shear stress $\overline{u'v'}$ with negative value is similar to $\overline{v'w'}$ in the CV. Comparing the distributions of different shear stresses in the CV, we found that $|\overline{u'w'}| \geq |\overline{u'v'}| > |\overline{v'w'}|$ for

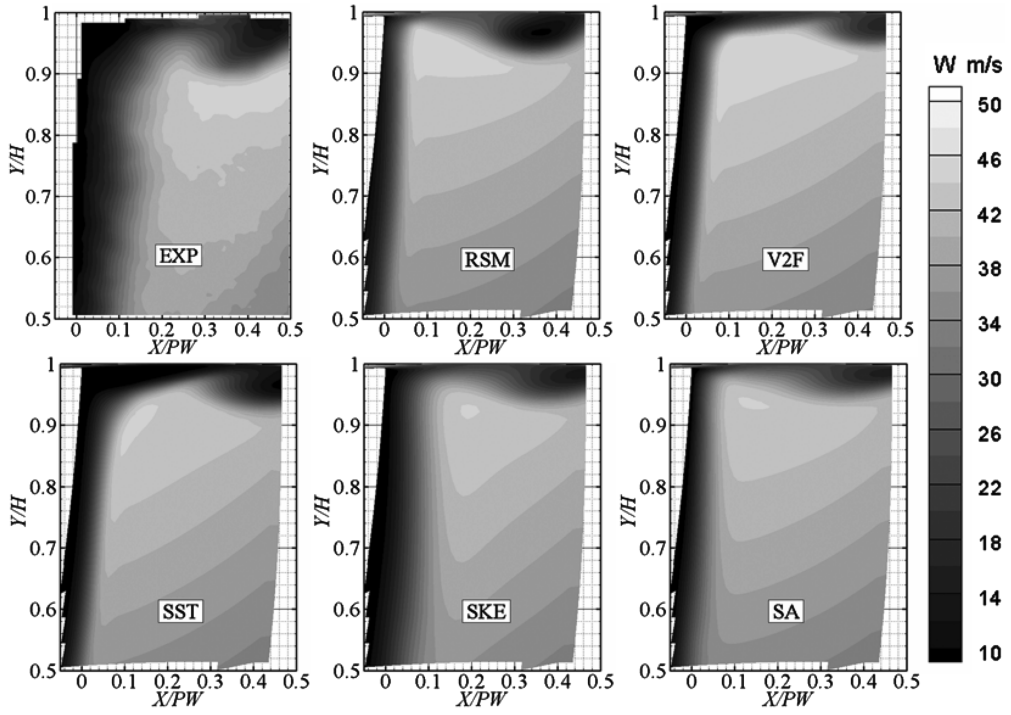

Fig. 12 Streamwise velocity at 70% chord for the near-stall condition.

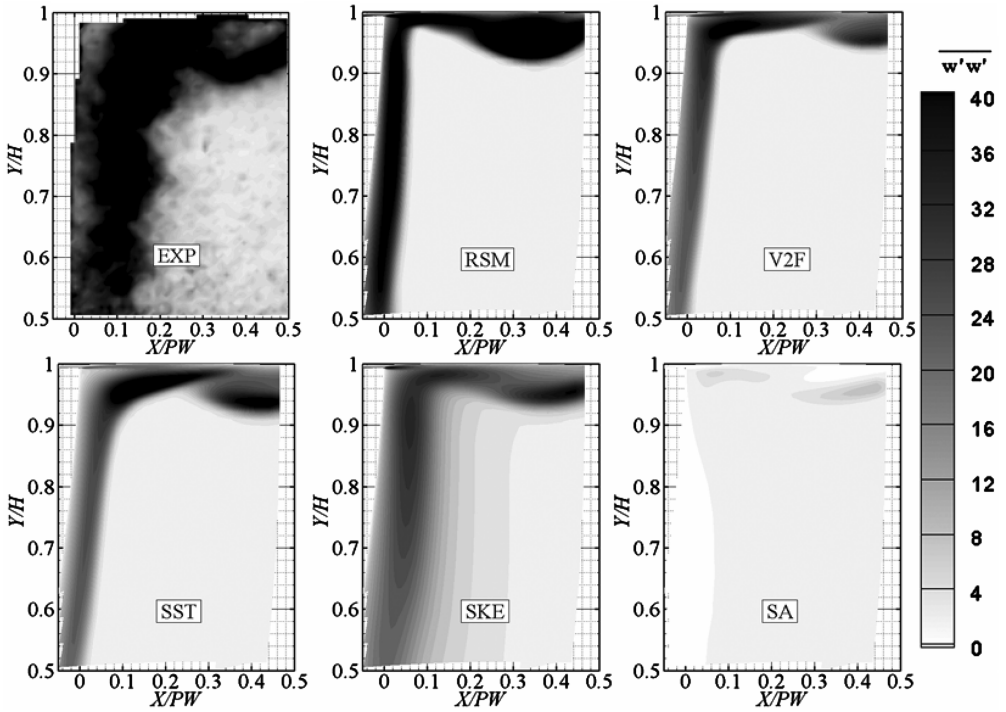

Fig. 13 Normal stress $\overline{w'w'}$ at 70% chord for the near-stall condition.

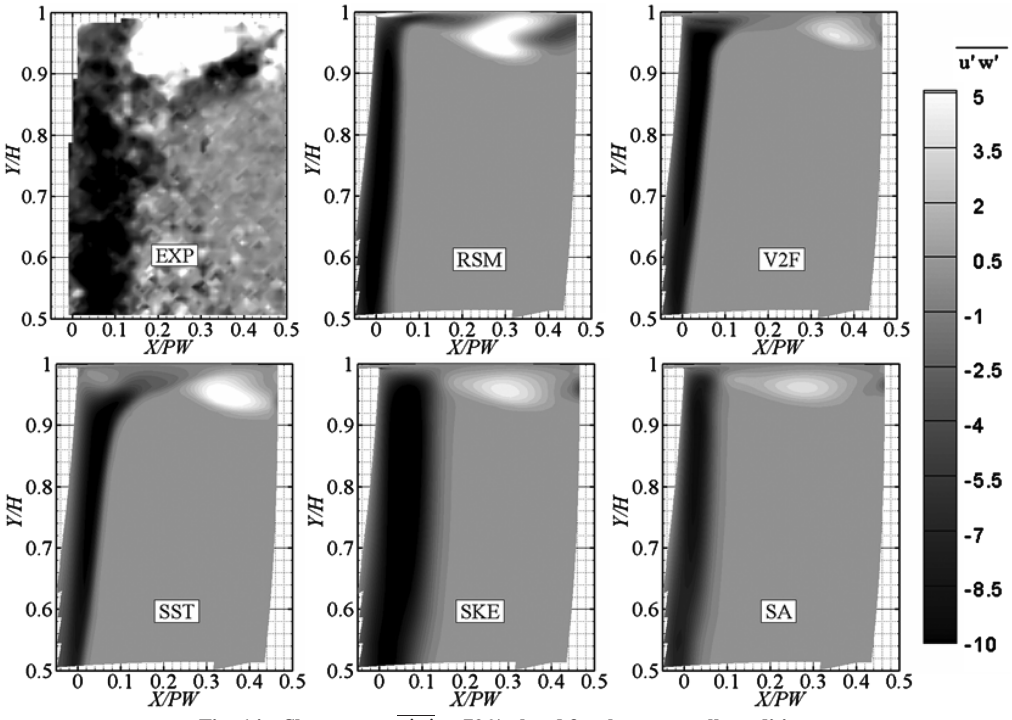

Fig. 14 Shear stress $\overline{u'w'}$ at 70% chord for the near-stall condition.

measurement, $|\overline{u'w'}| \geq 2|\overline{u'v'}| > |\overline{v'w'}|$ for the predictions with RSM, and $|\overline{u'w'}| \geq 2|\overline{u'v'}| \gg |\overline{v'w'}|$ for the predictions with the other models.

At other sections in the tip region, the turbulence stresses have similar distributions and the normal stresses are always higher than the shear stresses in the CV.

C. Discussion

The distribution of the streamwise velocity not only reveals the structures of the TLV and the CV, but also has a major effect on the rotor performance. Therefore, the streamwise velocity is selected as an example of a key factor for successful computation of the large-scale vortices in a compressor rotor.

The streamwise momentum equation for incompressible flow is as follows:

$$\frac{\mathrm{D}w}{\mathrm{D}t} = -\frac{1}{\rho}\frac{\partial p}{\partial z} + \nu\left(\frac{\partial^2 w}{\partial x^2} + \frac{\partial^2 w}{\partial y^2} + \frac{\partial^2 w}{\partial z^2}\right) + \underbrace{\frac{\partial(-\overline{u'w'})}{\partial x}}_{(1)} + \underbrace{\frac{\partial(-\overline{v'w'})}{\partial y}}_{(2)} + \underbrace{\frac{\partial(-\overline{w'w'})}{\partial z}}_{(3)} \tag{2}$$

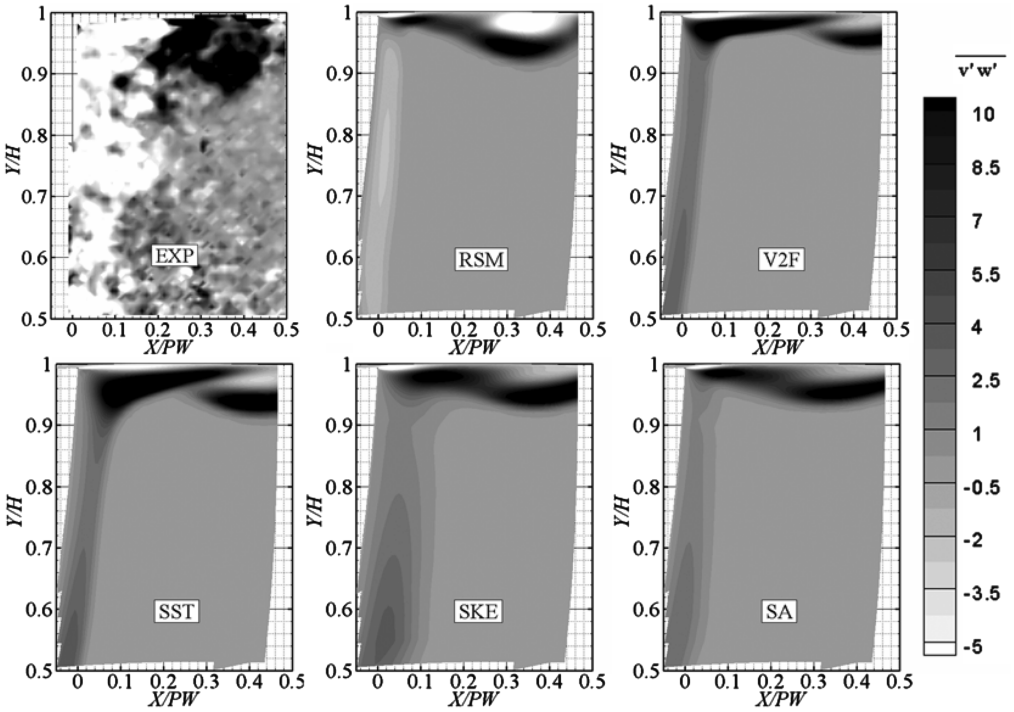

Fig. 15 Shear stress $\overline{v'w'}$ at 70% chord for the near-stall condition.

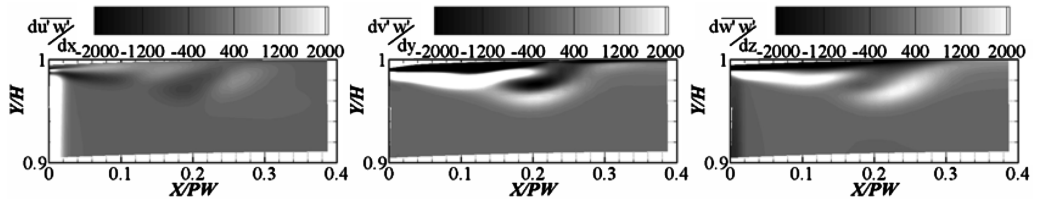

Fig. 16 Gradients of stresses at 60% chord for the design condition predicted by RSM.

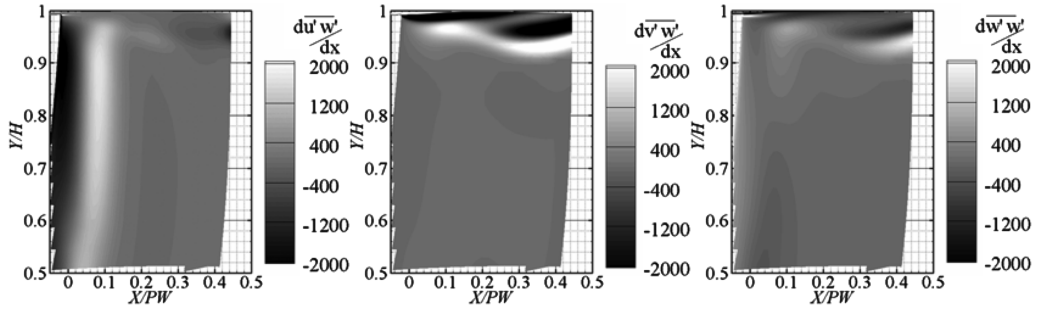

Fig. 17 Gradients of stresses at 70% chord for the near-stall condition predicted by SKE.

From the preceding equation, it is evident that the gradients of turbulence stresses are directly responsible for the variation of the streamwise velocity. An attempt is made to evaluate the relative magnitudes of the various terms presented in the preceding equation, to determine which of these terms are important in the TLV and CV. Because not all of the stresses can be derived from the SPIV measurements, term 1 to term 3 at the 60% chord for the design condition shown in Fig. 16 and at the 70% chord for the near-stall condition are derived from the best prediction results.

Figure 16 indicates that term 1 makes little contribution to the prediction of the TLV, whereas term 2 and term 3 make the primary contribution. Figure 17 indicates that term 1 makes a primary contribution to the prediction of the CV, whereas term 3 makes some contribution and term 2 only makes a little contribution. This is why SA can give nearly the same results as other models, though it always markedly underestimates the normal stresses. Therefore, in general, it could be concluded that correct calculation for the primary terms of the turbulence stresses is a key factor for the accurate prediction of the large-scale tip vortices in compressors.

V. Conclusions

Because of the main weakness of the turbulence model, the tip flows with complex large-scale vortices, such as the tip-leakage vortex and corner vortex, are still a big challenge for numerical simulations, especially for the steady CFD techniques used in the fan and compressor design routine nowadays and in the near future. To study the predictive capabilities of the different mature turbulence models for the large-scale vortices in the compressor rotor, the computation results of six turbulence models, including the mixing-length model, the Spalart–Allmaras model, the standard $k-\varepsilon$ model, the SST $k-\omega$ model, the $\overline{v^2}-f$ model, and the Reynolds stress

model, are carefully discussed and compared with the SPIV measurements both in terms of velocity fields and turbulence characteristics in the study. The following conclusions are drawn from these comparisons, which are more suitable for steady computations of subsonic compressors:

1) For the computation of the complicated flow structures in compressors, grid independence is better assessed based on the resolution of the flow structures that are of concern, such as the tip-leakage vortex in the present study, compared with looking only at the operating characteristics.

2) For the prediction of the tip-leakage vortex, the Reynolds stress model is shown to be superior to the other models at the design condition; at the near-stall condition, the structure and strength of the tip-leakage vortex predicted by the Reynolds stress model is still the best; and the circumferential motion of the tip-leakage vortex predicted by the $\overline{v^2} - f$ model and the SST $k - \omega$ model show more agreement with the measurement. For the prediction of the corner vortex at the near-stall condition, the standard $k - \varepsilon$ model gives the best results, whereas all other models underestimate the corner vortex in scale.

3) Normal stresses are much higher than shear stresses in both the tip-leakage vortex and corner vortex, whereas all models except the Spalart–Allmaras model could predict the characteristic; three components of the normal stresses are not in the same magnitude; and only the Reynolds stress model can predict this relationship, and it overestimates the streamwise normal stress $\overline{w'w'}$ relative to other normal stresses. It is also found that all models except the Reynolds stress model fairly underestimate shear stress $\overline{u'w'}$ in the tip-leakage vortex and $\overline{v'w'}$ in the corner vortex.

4) Although the simulation could predict the large-scale tip vortices well in the mean flowfield, the computed flow mechanism has large discrepancy with the reality. In the steady simulations, all of the turbulence models fail to account for the nonlinear effects of the tip-leakage vortex splitting and breakdown, as well as the compound vortex of the corner vortex.

Acknowledgments

The authors would like to acknowledge the support of National Natural Science Foundation of China, grants 50006001 and 50476001, and the support of the National Basic Research Program of China, grant 2007CB210103. The authors would also like to thank Aeroengine Simulation Research Center of the Beijing University of Aeronautics and Astronautics for the use of the FLUENT code.

References

[1] Denton, J. D., "Loss Mechanisms in Turbomachines," *Journal of Turbomachinery*, Vol. 115, No. 4, 1993, pp. 621–656.

[2] Storer, J. A., and Cumpsty, N. A., "An Approximate Analysis and Prediction Method for Tip Clearance Loss in Axial Compressors," American Society of Mechanical Engineers, Paper 93-GT-140, 1993.

[3] Adamczyk, J. J., Celestina, M. L., and Greitzer, E. M., "The Role of Tip Clearance in High-Speed Fan Stall," *Journal of Turbomachinery*, Vol. 115, No. 1, 1993, pp. 28–39.

[4] Rains, D. A., "Tip Clearance Flows in Axial Flow Compressors and Pumps," California Inst. of Technology, Hydrodynamics and Mechanical Engineering Labs., Rept. 5, Pasadena, CA, June 1954.

[5] Lakshminarayana, B., "Methods of Predicting the Tip Clearance Effects in Axial Flow Turbomachinery," *Journal of Basic Engineering*, Vol. 112, Sept. 1970, pp. 609–617.

[6] Chen, G. T., Greitzer, E. M., Tan, C. S., and Marble, F. E., "Similarity Analysis of Compressor Tip Clearance Flow Structure," *Journal of Turbomachinery*, Vol. 113, No. 2, 1991, pp. 260–271.

[7] Kang, S., and Hirsch, C., "Experiment Study on the Three-Dimension Flow Within a Compressor Cascade with Tip Clearance, Part 1: Velocity and Pressure Fields," *Journal of Turbomachinery*, Vol. 115, No. 3, 1993, pp. 444–452.

[8] Inoue, M., and Kurou, M., "Structure of Tip Clearance Flow in an Isolated Axial Compressor Rotor," *Journal of Turbomachinery*, Vol. 111, No. 3, 1989, pp. 250–256.

[9] Stauter, R. C., "Measurement of the Three-Dimensional Tip Region Flow Field in an Axial Compressor," *Journal of Turbomachinery*, Vol. 115, No. 3, 1993, pp. 468–476.

[10] Lakshminarayana, B., Zaccaria, M., and Marathe, B., "The Structure of Tip Clearance Flow in an Axial Flow Compressor," *Journal of Turbomachinery*, Vol. 117, No. 3, 1995, pp. 336–347.

[11] Foley, A. C., and Ivey, P. C., "Measurement of Tip-Clearance Flow in a Multistage, Axial Flow Compressor," *Journal of Turbomachinery*, Vol. 118, No. 2, 1996, pp. 211–217.

[12] Wernet, M. P., Zante, D. V., Strazisar, T. J., John, W. T., and Prahst, P. S., "3-D Digital PIV Measurements of the Tip Clearance Flow in an Axial Compressor," American Society of Mechanical Engineers, Paper GT-2002-30643, 2002.

[13] Liu, B. J., Wang, H. W., Liu, H. X., Yu, H. J., Jiang, H. K., and Chen, M. Z., "Experimental Investigation of Unsteady Flow Field in the Tip Region of an Axial Compressor Rotor Passage at Near Stall Condition with Stereoscopic Particle Image Velocimetry," *Journal of Turbomachinery*, Vol. 126, No. 3, 2004, pp. 360–374. doi:10.1115/1.1748367

[14] Liu, B. J., Yu, X. J., Liu, H. X., Jiang, H. K., and Chen, M. Z., "Evolution of the Tip Leakage Vortex in an Axial Compressor Rotor," American Society of Mechanical Engineers, Paper 2004-GT-53703, 2004.

[15] Inoue, M., Furukawa, M., Saiki, K., and Yamada, K., "Physical Explanations of Tip Leakage Flow Field in an Axial Compressor Rotor," American Society of Mechanical Engineers, Paper 98-GT-91, 1998.

[16] Inoue, M., Kuroumaru, M., Yoshida, S., Minami, T., Yamada, K., and Furukawa, M., "Effect of Tip Clearance on Stall Evolution Process in a Low-Speed Axial Compressor Stage," American Society of Mechanical Engineers, Paper GT-2004-53354, 2004.

[17] Gerolymos, G. A., and Vallet, I., "Tip-Clearance and Secondary Flows in a Transonic Compressor Rotor," *Journal of Turbomachinery*, Vol. 121, No. 4, 1999, pp. 751–762.

[18] Furukawa, M., Inoue, M., Saiki, K., and Yamada, K., "The Role of Tip Leakage Vortex Breakdown in Compressor Rotor Aerodynamics," *Journal of Turbomachinery*, Vol. 121, No. 3, 1999, pp. 469–480.

[19] Furukawa, M., Saiki, K., Yamada, K., and Inoue, M., "Unsteady Flow Behavior Due to Breakdown of Tip Leakage Vortex in an Axial Compressor Rotor at Near Stall Condition," American Society of Mechanical Engineers, Paper 2000-GT-0666, 2000.

[20] Bae, J., Breuer, K. S., and Tan, C. S., "Control of Tip Clearance Flows in Axial Compressors," AIAA Paper 2000-2233, 2000.

[21] Bae, J., Breuer, K. S., and Tan, C. S., "Active Control of Tip Clearance Flow in Axial Compressors," *Journal of Turbomachinery*, Vol. 127, No. 2, 2005, pp. 352–362. doi:10.1115/1.1776584

[22] Glanville, J. P., "Investigation into Core Compressor Tip Leakage Modeling Techniques Using a 3D Viscous Solver," American Society of Mechanical Engineers, Paper 2001-GT-0336, 2001.

[23] Van Zante, D. E., Strazisar, A. J., Wood, J. R., Hathaway, M. D., and Okiishi, T. H., "Recommendations for Achieving Numerical Simulation of Tip Clearance Flows in Transonic Compressor Rotors," *Journal of Turbomachinery*, Vol. 122, No. 4, 2000, pp. 733–742. doi:10.1115/1.1314609

[24] Gupta, A., Khalid, S. A., McNulty, G. S., and Dailey, L., "Prediction of Low Speed Compressor Rotor Flow Fields with Large Tip Clearances," American Society of Mechanical Engineers, Paper GT-2003-38637, 2003.

[25] Lee, G. H., Park, J., and Baek, J. H., "Performance Assessment of Turbulence Models for the Quantitative Prediction of Tip Leakage Flow in Turbomachines," American Society of Mechanical Engineers, Paper GT-2004-53403, 2004.

[26] Liu, B. J., Yu, X. J., Liu, H. X., Jiang, H. K., Yuan, H. J., and Xu, Y. T., "Application of SPIV in Turbomachinery," *Experiments in Fluids*, Vol. 40, 2006, pp. 621–642. doi:10.1007/s00348-005-0102-9

[27] Basson, A. H., and Lakshminarayana, B., "Numerical Simulation of Tip Clearance Effects in Turbomachinery," *Journal of Turbomachinery*, Vol. 117, 1995, pp. 348–359.

[28] Dener, C., and Hirsch, Ch., "IGG: An Interactive 3D Surface Modeling and Grid Generation System," AIAA Paper 92-0037, 1992.

[29] *FLUENT 6.0 User's Guide*, FLUENT Inc., Lebanon, NH, 2002.

[30] Wilcox, D. C., *Turbulence Modeling for CFD*, 2nd ed., DCW Industries, La Cãnada, CA, 2000, pp. 49–79.

[31] Spalart, P., and Allmaras, S., "A One-Equation Turbulence Model for Aerodynamic Flows," AIAA Paper 92-0439, 1992.

[32] Launder, B. E., and Spalding, D. B., *Lectures in Mathematical Models of Turbulence*, Academic Press, London, 1972.

[33] Menter, F. R., "Two-Equation Eddy-Viscosity Turbulence Models for Engineering Applications," *AIAA Journal*, Vol. 32, No. 8, 1994, pp. 1598–1605.
[34] Durbin, P. A., "Separated Flow Computations with the $k-\varepsilon-v^2$ Model," *AIAA Journal*, Vol. 33, No. 4, 1995, pp. 659–664.
[35] Launder, B. E., Reece, G. J., and Rodi, W., "Progress in the Development of a Reynolds-Stress Turbulence Closure," *Journal of Fluid Mechanics*, Vol. 68, No. 3, 1975, pp. 537–566. doi:10.1017/S0022112075001814
[36] Chakraborty, P., Balachandar, S., and Adrian, A. J., "On the Relationships Between Local Vortex Identification Schemes," *Journal of Fluid Mechanics*, Vol. 535, July 2005, pp. 189–214. doi:10.1017/S0022112005004726

F. Liu
Associate Editor